Effect of spatial and temporal variations of the boundary temperature on the thermal stability of horizontal flows

Olaf Stiller,[1] Wolfgang Schöpf,[2] John C. Patterson,[2] and Andrew Schultz[2]
[1]*Department of Meteorology, University of Reading, Earley Gate, Reading RG6 6BB, United Kingdom*
[2]*Department of Civil and Environmental Engineering, James Cook University of North Queensland, Townsville, Queensland 4811, Australia*
(Received 22 December 1997)

The effects of linear spatial and temporal variations of the boundary temperature on the thermal instability are discussed for different types of horizontal flows, which typically consist of forced and temperature-induced velocity components. The nonlinear temperature profile resulting from such boundary conditions leads to an unstable layer of height h_u, even when the fluid as a whole is heated from above. The critical values of the Rayleigh and the wave number, defined with respect to this unstable layer, differ in most cases only little from their asymptotic values for $h_u \to 0$. The temperature-induced velocity component may be stabilizing or destabilizing, depending on whether h_u is large or small. A temporal increase (decrease) of the boundary temperature has a destabilizing (stabilizing) influence if the unstable layer is in the lower part of the channel, and the opposite effect if it is in the upper part. These results are compared to the considerably different situation when a constant heat flux is imposed at the boundaries. The instability's Prandtl number dependence, which results from the coupling between the horizontal temperature gradient and the shear of the velocity field, is discussed in terms of energy considerations. [S1063-651X(98)14205-8]

PACS number(s): 47.27.Te, 44.25.+f, 47.15.−x, 47.20.Bp

I. INTRODUCTION

A horizontal parallel flow that is homogeneously heated from below becomes unstable with respect to thermal convection when the applied temperature difference exceeds a certain critical value. It is well known that the threshold and the critical wavelength of this instability are the same as for the classical Rayleigh-Bénard problem. The through-flow merely acts as a selection mechanism for the direction of the wave vector in that the resulting convection rolls are parallel to the flow direction [1,2]. The stability properties change drastically, however, if in addition to the vertical variations also horizontal or temporal temperature variations leading to nonlinear vertical temperature profiles are included. Most of the earlier work on this topic was restricted to closed flows, such as flows in closed containers (see Refs. [3,4]). Studies of a Poiseuille flow, on the other hand, were largely based on the assumption that the velocity field is not altered by the horizontal temperature gradient, and thus covered only a very limiting case [5]. Correspondingly, the theoretical predictions overestimated the threshold for large heat advection where, as explained below, the neglected temperature-induced flow in fact leads to an additional destabilization. The more recent analysis of Ref. [6] focused on open flows that are forced by a horizontal pressure gradient Δp_x through channels with constant heat flux at the horizontal boundaries. In that case, the thermal instability is triggered by an unstable layer of height h_u which is caused by the nonlinear temperature profile. It was found that a Rayleigh number Ra^u defined with respect to this unstable layer has similar critical values for very different flow types, while the critical values of the usual Rayleigh number Ra (defined with respect to the total channel height) would vary over many orders of magnitude [6].

The present paper deals with the corresponding but in many respects quite different results for systems where spatial and/or temporal temperature variations are imposed by perfectly conducting horizontal boundaries [7]. The methods and notations are largely the same as in Ref. [6]. In Sec. II, the fundamental hydrodynamic equations are presented, and in Sec. III the base flows resulting from these equations are derived and discussed for the system under consideration. It is shown that the velocity field is a superposition of a forced and a temperature-induced component, the latter being caused by the horizontal temperature gradient. The corresponding vertical temperature profile is nonlinear and can be separated into four parts, two of which are induced by the two parts of the velocity field while the other two result from the time-dependent and time-independent parts of the boundary condition. Also in Sec. III, the conditions under which such a temperature profile will lead to a potentially unstable layer are derived, and the influence of the temperature-induced flow component as well as the influence of temporal temperature changes on this layer are discussed in detail. A linear stability analysis of these flows is presented in Sec. IV, with the results being discussed in Sec. V. It turns out that, similar to the case of constant heat flux boundaries [6], the instability is indeed triggered by an unstable layer of height h_u. The Rayleigh number Ra^u and wave number k^u, both defined with respect to h_u, have critical values that depend only on the unstable layer and its neighborhood, and which for sufficiently small h_u are largely independent of the explicit value of h_u. In the usual Rayleigh-Bénard system, the source of instability is easily identified as the negative vertical temperature gradient, leading to critical Rayleigh and wave numbers that are Prandtl number independent. The equations presented in Sec. IV, however, exhibit a second possible instability mechanism that results from the coupling

between the horizontal temperature gradient β and the vertical shear $\partial_z \overline{U}$ of the velocity profile. This mechanism is Prandtl number dependent. Qualitative arguments for its influence are given in Sec. IV and are confirmed in Sec. V, where the results for Pr=7 are compared to those for Pr $\rightarrow\infty$.

II. BASIC EQUATIONS

The parallel flows considered here are assumed to be of infinite horizontal extent in the x-y plane and are driven by a horizontal pressure gradient Δp_x. In the vertical z direction, they are bounded by two perfectly conducting, no-slip boundaries (at $z=\pm H$) with temperatures $T(z=\pm H)=\mp\Delta T/2+\beta x+c_b t+\text{const}$. These boundaries impose a vertical temperature difference ΔT, a horizontal temperature gradient β, and temperature changes in time with a constant rate c_b. Defining $U_0=-c_b/\beta$ and using an appropriate nondimensionalization, the boundary condition can be written as

$$T(z=\pm 1)=\mp\frac{\Delta T}{2}+\beta(x-U_0 t)+\text{const}, \tag{1}$$

thus showing that the time dependence of the boundaries vanishes when observed from a frame of reference that moves with U_0. Space, time, and temperature are scaled in units of H, H^2/ν, and $\nu^2/(g\alpha H^3)$, respectively. H is half the channel height, g is the acceleration due to gravity, α is the coefficient of thermal expansion, and ν is the kinematic viscosity. The constant in Eq. (1) will be suppressed in the following as only temperature differences are important.

We will consider parallel flows of the general form

$$U=\overline{U}(z), \quad V=W=0, \tag{2a}$$

$$T=\overline{T}(z)+\beta(x-U_0 t), \tag{2b}$$

where U and V are the horizontal and W the vertical velocity components. The profiles $\overline{U}(z)$ and $\overline{T}(z)$ have to be derived from the Navier-Stokes equations and the heat equation, which in the Boussinesq approximation read (translational invariance is assumed in the y direction)

$$(\partial_t+U\partial_x+W\partial_z)U=-\partial_x P+\nabla^2 U, \tag{3a}$$

$$(\partial_t+U\partial_x+W\partial_z)W=-\partial_z P+\nabla^2 W+T, \tag{3b}$$

$$\mathrm{Pr}(\partial_t+U\partial_x+W\partial_z)T=\nabla^2 T. \tag{3c}$$

$\mathrm{Pr}=\nu/\kappa$ is the Prandtl number with κ the thermal diffusion. As in Ref. [6], we mainly consider Pr=7, as appropriate for water.

Inserting Eqs. (2a) and (2b) into Eq. (3b) yields $0=-\partial_z P+T$ and thus $\partial_x P=\int \partial_x T dz+\Delta p_x=\beta z+\Delta p_x$. By using this to eliminate the pressure from Eq. (3a) and then inserting Eqs. (2a) and (2b) into Eqs. (3a) and (3c), we finally obtain

$$\partial_z^2 \overline{U}=\beta z+\Delta p_x, \tag{4a}$$

$$\partial_z^2 \overline{T}=\mathrm{Pr}\beta(\overline{U}-U_0). \tag{4b}$$

III. BASE FLOW

The velocity field can be derived from Eq. (4a) as a superposition of a temperature-induced flow proportional to β (and with zero average) and a Poiseuille flow forced by the constant horizontal pressure gradient Δp_x (with an average velocity $v_m=-\Delta p_x/3$):

$$\overline{U}(z)=\beta U_\beta(z)+v_m U_p(z). \tag{5}$$

Using the no-slip boundary condition $\overline{U}(z=\pm 1)=0$, we find $U_\beta(z)=z(z^2-1)/6$ and $U_p(z)=(3/2)(1-z^2)$. Equation (4b) together with the boundary condition (1) then yields the temperature profile as

$$\overline{T}(z)=\mathrm{Pr}\beta v_m\left(T_p(z)-\frac{U_0}{v_m}\frac{z^2}{2}+\frac{\beta}{v_m}T_\beta(z)\right)-\frac{\Delta T}{2}z, \tag{6}$$

where

$$\partial_z^2 T_p=U_p(z) \quad \text{and} \quad \partial_z^2 T_\beta=U_\beta(z).$$

We choose $T_p(+1)=T_p(-1)$ and $T_\beta(+1)=T_\beta(-1)$, so that the net temperature difference across the channel is entirely determined by the last term $\Delta T z/2$ on the right-hand side of Eq. (6), and hence find $T_p(z)=z^2(3-z^2/2)/4$ and $T_\beta(z)=z(z^4/10-z^2/3+7/30)/12$. ($T_\beta$ here differs by a term $z/45$ from the corresponding function in Ref. [6]).

Obviously, Eqs. (4a) and (4b) can also be solved for more general types of forced flows with the form of Eqs. (5) and (6) remaining unchanged, provided that the forced velocity component $U_p(z)$ and the corresponding temperature component $T_p(z)$ are adjusted properly. For a Couette flow, i.e., a flow with moving upper and nonmoving lower boundary as well as $\Delta p_x=0$ in Eq. (4a), we find $U_p(z)=(z+1)$ and $T_p(z)=z^2/2+z(z^2-1)/6$. In Sec. V, the systematics of our approach will be illustrated by comparing the results for flows with nonmoving boundaries to those for ''pure Couette flow,'' i.e., Couette flow with $\beta\ll v_m$, where the temperature-induced flow can be neglected and the velocity profile is indeed linear.

For discussing the relevance of the different terms in Eq. (6), β and v_m are assumed to be positive [8]. This leads to a potentially unstable layer at the bottom boundary when $\Delta T/(\beta v_m)$ exceeds a certain value. The necessary condition $\partial_z \overline{T}(z=-1)<0$ for the existence of such a layer yields by evaluating Eq. (6)

$$\frac{\Delta T}{2\mathrm{Pr}\beta v_m}>-1+\frac{U_0}{v_m}-\frac{1}{45}\frac{\beta}{v_m}. \tag{7}$$

It is interesting to note that unstable situations arise even when the temperature difference over the whole channel would favor stability, i.e., for $\Delta T<0$. This is caused by the nonlinear part of $\overline{T}(z)$, the magnitude of which is given by the overall prefactor in Eq. (6), i.e., by the average heat advection βv_m. Therefore, increasing the value of βv_m will in most cases increase the instability.

The temperature profiles in Figs. 1(b), 2(b), and 3 illustrate the criterion (7) for different values of $\Delta T/(2\mathrm{Pr}\beta v_m)$, which decreases from left to right, i.e., from more to less unstable. Figure 1 corresponds to the simplest case $U_0=0$

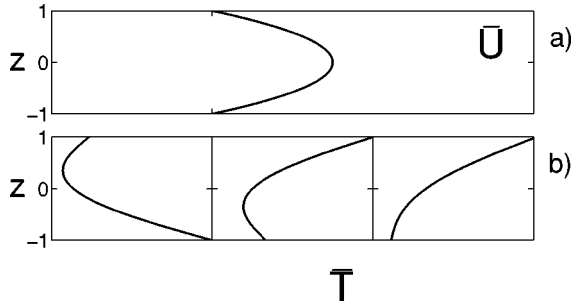

FIG. 1. (a) Velocity profile $\bar{U}(z)$ and (b) corresponding temperature profiles $\bar{T}(z)$ for $U_0=0$ and $\beta/v_m \ll 1$ fixed. The different curves in (b) correspond from left to right to the different values of $\Delta T/(2\mathrm{Pr}\beta v_m)=0.5,-0.5,-1.2$, i.e., from more to less unstable [compare Eq. (7)].

and $\beta/v_m \ll 1$, where the velocity field is the same as for ordinary Poiseuille flow. The decrease of the height of the unstable layer and its eventual disappearance are obvious in Fig. 1(b) from left to right. Figures 2 and 3 demonstrate how the profiles shown in Fig. 1 are influenced by the β-induced flow and by temporal temperature variations, respectively. These cases will be discussed in more detail below. It will be assumed that the onset of thermal instability is predominantly determined by the strength of the unstable layer. The influence of the different terms is expected to be stabilizing when they increase the temperature gradient in the unstable region and its neighborhood (i.e., decrease $-\partial_z\bar{T}$), and destabilizing when they decrease the temperature gradient (increase $-\partial_z\bar{T}$) there [9]. This approach is justified by the results of the stability analysis presented in Sec. V.

A. Influence of the temperature-induced flow

The individual temperature profiles shown in the three subsets on the right-hand side of Fig. 2(b) all have $U_0=0$. They are induced by the velocity profiles shown in the right subset of Fig. 2(a), which are for different values of β/v_m with the average heat advection βv_m being held constant. Note that an increase of β/v_m increases the contribution of T_β to the temperature profile [see Eq. (6)], and that the derivative of T_β is positive in the middle part of the channel and negative near the boundaries. Correspondingly, an increase of β/v_m is destabilizing when h_u is small or zero [see the third and fourth subset of Fig. 2(b)], whereas it has a stabilizing effect when the potentially unstable layer extends well over the middle part of the channel. In the latter case, it decreases the height h_u of the unstable layer as well as the temperature difference ΔT_u across it, as can be seen in the second subset of Fig. 2(b).

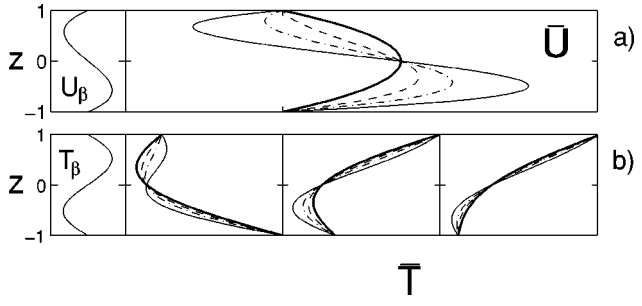

FIG. 2. (a) Velocity and (b) temperature profiles for $U_0=0$ and different values of β/v_m. The bold lines are the same as in Fig. 1, i.e., for $\beta/v_m \ll 1$. The thin dashed, thin dashed-dotted, and thin solid lines are for $\beta/v_m=8,16,32$, respectively. Different curves in each of the 4 subsets on the right differ from each other only by a multiple of the function shown in the left part of the respective row.

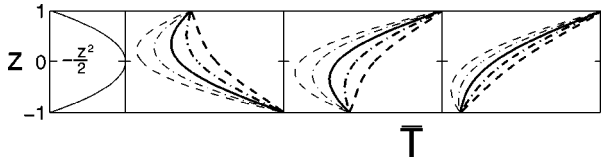

FIG. 3. Vertical temperature profiles for $\beta/v_m \ll 1$ fixed and different values of U_0/v_m. The solid lines are the same as in Fig. 1(b), i.e., for $U_0=0$. The thin dashed, thin dashed-dotted, bold dashed-dotted, and bold dashed lines are for $U_0/v_m=-0.8$, $-0.4,0.4,0.8$, respectively. Different curves in each of the 3 subsets on the right differ from each other only by a multiple of the function shown in the left subset.

Our analysis explains why in an earlier study for conducting boundaries, where the influence of T_β has been neglected [5], the theory overestimated the measured threshold for the case of large horizontal heat advection. Apparently, the experimental flow had a substantial β-induced component that, as explained above, will lower the threshold for small h_u. [Note that large heat advection corresponds to small h_u, since it leads to a strongly curved vertical temperature profile, see Eq. (4b)]. This behavior is in contrast to the case of boundaries with constant heat flux, where the contribution coming from the temperature-induced flow component is stabilizing everywhere in the channel [6] (see also Fig. 4). In that case, an increase of the temperature-induced flow decreases the temperature difference $\Delta T=T(-1)-T(+1)$ across the channel.

B. Influence of temporal temperature variations

The temporal variations of the boundary temperature included in Eq. (1) have no influence on the velocity profile, however, they alter the vertical temperature profile by adding a term proportional to $-z^2/2$ [see Eq. (6)]. As seen on the left-hand side of Fig. 3, this has a stabilizing effect in the lower and a destabilizing effect in the upper part of the channel. Since the flows considered here have their unstable region at the bottom of the channel, it is the behavior in this lower region that determines the instability, at least for not

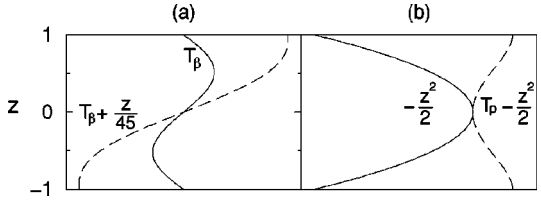

FIG. 4. (a) β-induced component of $\bar{T}(z)$ for conducting (solid line: T_β) and constant heat flux boundaries (dashed line: $T_\beta+z/45$). (b) The component of $\bar{T}(z)$ induced by temporal temperature variations for conducting (solid line: $-z^2/2$) and constant heat flux boundaries (dashed line: $T_p-z^2/2$ [10]).

too large h_u. The three subsets on the right-hand side of Fig. 3 demonstrate this behavior for different values of $\Delta T/\beta v_m$. We generally find that $U_0<0$ is destabilizing and $U_0>0$ is stabilizing, except for very large values of U_0/v_m when the term proportional to $-z^2/2$ creates an unstable region in the upper part of the channel (not shown here). In the last subset of Fig. 3, one can particularly observe how an unstable layer (which does not exist for $U_0=0$, bold solid line) is formed for $U_0<0$ (thin lines), i.e., by a linear temporal increase of the boundary temperature. In the second subset from the right, the unstable layer for $U_0=0$ (bold solid line) disappears for sufficiently large $U_0/v_m>0$ (bold dashed line).

In channels with constant boundary heat flux, it was found that temporal temperature changes have the opposite effect [6]. In that case, a linear temperature decrease ($\beta U_0>0$) is destabilizing for flows with $\beta/v_m \ll 1$, because temporal temperature variations ($U_0\neq 0$) change the prefactor βv_m of the nonlinear part of $\overline{T}(z)$ in Eq. (6). As shown in the Appendix, the effect on βv_m can be combined with the term proportional to $-z^2/2$ to form an effective temperature component $T_p-z^2/2$, which largely describes the influence of temporal temperature variations for constant heat flux boundaries [10]. As seen in Fig. 4(b), this component has the opposite stability characteristics as $-z^2/2$.

In order to gain an intuitive understanding of these different behaviors, note that for constant heat flux boundaries, situations with $\beta U_0>0$ may result from linearly decreasing the fluid temperature at the inflow of the channel so that the time dependence of the temperature inside the channel is a consequence of heat advection (bulk heating) alone (see also Ref. [6]). Therefore, the bottom layer is in some way effectively cooled from *above*, since advective heat transport is stronger in the middle of the channel where the flow velocity is larger. For conducting boundaries on the other hand, $\beta U_0>0$ is caused by decreasing the temperature at the boundaries, which means an effective cooling from *below*, since the bottom boundary will have a larger impact on the bottom layer than the upper boundary.

IV. LINEAR STABILITY ANALYSIS

A. Eigenvalue equations

We now perform a linear stability analysis of the basic solutions discussed above with respect to longitudinal stationary thermal convection modes [1,2]. These modes are x independent and of the form $F(z)\exp(iky+\sigma t)$, with the real numbers k and σ being the wave number and the growth rate and $F(z)$ the eigenfunction. The fundamental equations linearized with respect to such perturbations yield the eigenvalue problem for $\sigma=\sigma(k)$. For an incompressible fluid ($\partial_x U+\partial_y V+\partial_z W=0$), these equations can be written as

$$(\sigma-\partial_z^2+k^2)\,\tilde{u}=-\beta\overline{U}'w, \tag{8a}$$

$$(\sigma-\partial_z^2+k^2)(\partial_z^2-k^2)w=-k^2\vartheta, \tag{8b}$$

$$(\mathrm{Pr}\sigma-\partial_z^2+k^2)\,\vartheta=-\mathrm{Pr}(\overline{T}'w+\tilde{u}), \tag{8c}$$

with the primes indicating derivatives with respect to z (e.g., $\overline{T}'=\partial_z\overline{T}$). $\overline{U}(z)$ and $\overline{T}(z)$ are given by Eqs. (5) and (6) above, ϑ is the temperature component of the perturbation, and u and w are the longitudinal and vertical velocity perturbations, with $\tilde{u}=\beta u$. If $\sigma(k)\leqslant 0$ for all wave numbers k, the flow is linearly stable. The wave number k_c for which $\sigma(k)$ first crosses the origin is the *critical* wave number, and the parameters where this occurs are the *critical* parameters.

B. Instability mechanisms

According to Eqs. (8a)–(8c), the thermal stability of the flow is determined by $\overline{T}'$ and $\beta\overline{U}'$ only. While the destabilizing effect of $\overline{T}'<0$ is well known from the usual Rayleigh-Bénard problem, the influence of $\beta\overline{U}'$ is less evident. From Eq. (4b) we find $\beta\overline{U}'=\mathrm{Pr}^{-1}\overline{T}'''$, so that the influence of the β-$\overline{U}'$ coupling increases with decreasing Pr. For large Pr it can be neglected, in which case Eq. (8a) decouples from Eqs. (8b) and (8c). The stability problem then becomes identical to the ''usual'' Rayleigh-Bénard problem (but still for a nonlinear vertical temperature profile) where the critical values are Pr independent.

In order to gain a qualitative understanding of the β-$\overline{U}'$ coupling, we consider the (generalized) energy integrals that are obtained by multiplying Eqs. (8a)–(8c) by u^*, w^*, and ϑ^*, respectively (the asterisk indicates the complex conjugate), and then integrating over z. The real parts of these equations can be written as

$$\langle\beta\overline{U}'\tilde{u}w^*\rangle=-\sigma\langle|\tilde{u}|^2\rangle-\langle|\nabla\tilde{u}|^2\rangle, \tag{9a}$$

$$k^2\langle w\vartheta^*\rangle=\sigma\langle|\nabla w|^2\rangle+\langle|\nabla^2 w|^2\rangle, \tag{9b}$$

$$\mathrm{Pr}\sigma\langle|\vartheta|^2\rangle=-\langle|\nabla\vartheta|^2\rangle-\mathrm{Pr}(\langle\overline{T}'w\vartheta^*\rangle+\langle\tilde{u}\vartheta^*\rangle). \tag{9c}$$

$\langle\ \rangle$ denotes the integral over the real part, and $\nabla=(\partial_x,\partial_y,\partial_z)$ with $\partial_x=ik$ and $\partial_y=0$ for the perturbations considered here. Equation (9a) implies that $\langle\beta\overline{U}'\tilde{u}w^*\rangle<0$ in a vicinity of the threshold. If we consider a situation where $\beta\overline{U}'>0$ then $\langle\beta\overline{U}'\tilde{u}w^*\rangle<0$ indicates that $\tilde{u}$ is negatively correlated to w. Since w and ϑ are positively correlated [$\langle w\vartheta^*\rangle>0$, see Eq. (9b)], $\tilde{u}$ is normally also negatively correlated to ϑ (i.e., $\langle\tilde{u}\vartheta^*\rangle<0$). Therefore, such a situation enhances temperature perturbations [see Eq. (9c)], so that $\beta\overline{U}'>0$ is expected to have a destabilizing effect, while $\beta\overline{U}'<0$ should be stabilizing.

Since the instability of the flows studied here is triggered by an unstable layer, we conclude that the perturbations are largest within this layer which therefore dominates the integrals in Eqs. (9a)–(9c). As a consequence, the net influence of the second, Prandtl number dependent mechanism on these flows is determined by the sign of $\beta\overline{U}'$ in this layer. In Sec. V below, we will show that the differences between the results for $\mathrm{Pr}=7$ and $\mathrm{Pr}\to\infty$ are indeed well explained by this argument.

V. RESULTS AND DISCUSSION

Some quantitative results of the stability calculations are shown in Figs. 5–8. The Rayleigh number Ra^u and the wave number k^u, which are used to characterize the thermal instability, are defined with respect to the unstable layer of height h_u and in our scales are given by

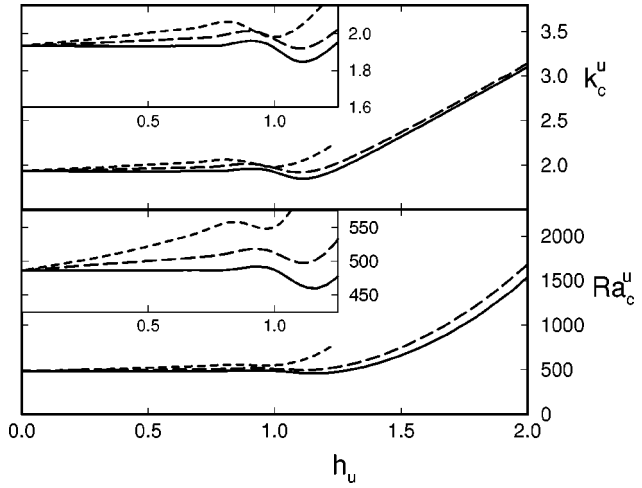

FIG. 5. Critical values Ra_c^u and k_c^u as functions of h_u for flows with $\mathrm{Pr}=7$ and $U_0=0$ (i.e., only spatial temperature variations). The solid and the long-dashed lines are for pure Couette and Poiseuille flows ($\beta/v_m \ll 1$), respectively, while the short-dashed lines are for $\beta/v_m=100$.

$$\mathrm{Ra}^u=\mathrm{Pr}h_u^3\Delta T_u$$

and

$$k^u=kh_u,$$

where ΔT_u is the temperature difference across this unstable layer. It turns out that the critical values Ra_c^u and k_c^u behave in a similar manner for very different flow types. Note that a large value of h_u corresponds to a comparably small curvature of $\overline{T}(z)$, which occurs for small βv_m and βU_0 [compare Eq. (6)]. In this regime, where Ra_c^u and k_c^u rise more rapidly (see Figs. 5–7), the critical value Ra_c of the usual Rayleigh number, defined with respect to the total channel height, changes more slowly and may thus yield a reasonable stability estimate [11]. For larger βv_m and/or βU_0, however, Ra_c would change its sign and vary over many orders of magnitude, so that it cannot be used for stability measures. Ra_c^u and k_c^u, on the other hand, vary rather slowly, and for $h_u \to 0$ they tend towards constant values that are the same for flows of completely different origins (the insets in Figs. 5 and 6 show this region in more detail).

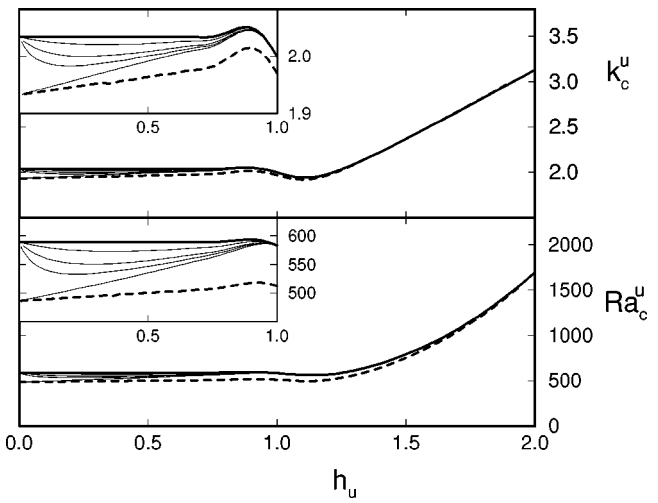

FIG. 6. Critical values Ra_c^u and k_c^u as functions of h_u for flows with temporal temperature variations (here $\mathrm{Pr}=7$ and $\beta/v_m \ll 1$). The bold solid lines are for $\beta=0$ (with βU_0 finite), and the thin lines are for $\Delta T/(2\mathrm{Pr}\beta v_m)=-1,-1.2,-1.5,-3$ from bottom to top. The bold dashed lines are the same as in Fig. 5, and are shown as a reference.

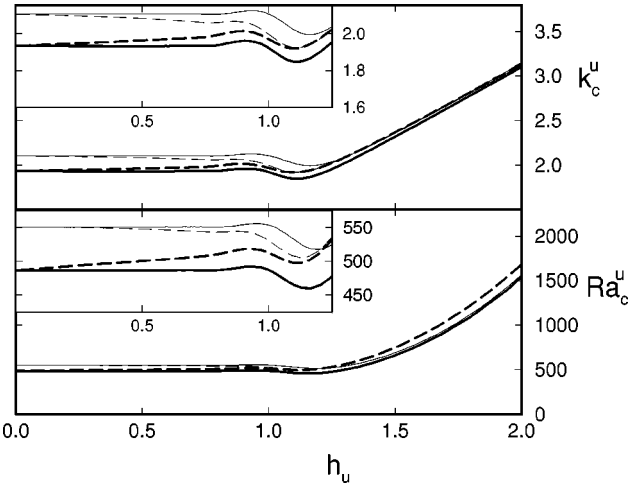

FIG. 7. Critical values Ra_c^u and k_c^u as functions of h_u for flows with different Prandtl numbers. The bold lines are the same as in Fig. 5 ($\mathrm{Pr}=7$; solid lines: Couette flow; dashed lines: Poiseuille flow). The thin lines show the corresponding results for $\mathrm{Pr}\to\infty$.

In Ref. [6], the behavior for small h_u was explained in terms of the scaling properties of the flow in the unstable region and its neighborhood. As h_u becomes small, $\overline{U}(z)$ may be approximated by a linear Couette flow $\overline{U}(z) \approx \overline{U}'(-1)(z+1)$ in this region, which, according to Eq. (4b), corresponds to

$$\overline{T}'(z) \approx \mathrm{Pr}\beta\left(\frac{\overline{U}'(-1)}{2}(z+1)^2-U_0(z+1)\right)+\Theta_l, \tag{10}$$

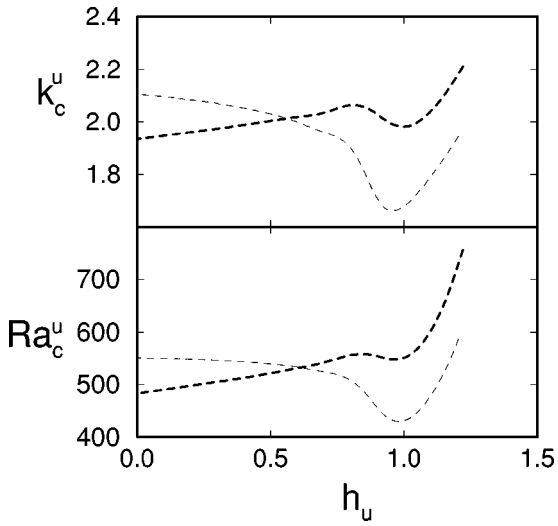

FIG. 8. Similar to Fig. 7, but now for a flow with $\beta/v_m=100$. The bold lines are the same as in Fig. 5 ($\mathrm{Pr}=7$), while the thin lines are for $\mathrm{Pr}\to\infty$.

where $\Theta_l = \partial_z \overline{T}(z=-1)$ is the heat flux at the lower boundary. In this approximation, the stability problem depends only on two scale-invariant parameters so that Ra_c^u and k_c^u are completely determined by the parameter $S_{\mathrm{inv}} = \mathrm{Pr}\beta U_0 h_u/\Theta_l$. In particular, all flows with $U_0=0$ (and thus $S_{\mathrm{inv}}=0$) have the same critical values in this limit. This behavior is demonstrated in Fig. 5 for Couette (solid lines) and Poiseuille flow (long-dashed lines) as well as for flows with a large β-induced velocity component ($\beta/v_m=100$, short-dashed lines).

Figure 6 shows the corresponding results for instabilities that are caused by a linear increase of the boundary temperature with time ($U_0/v_m<0$). The bold solid lines are for pure temporal, i.e., no horizontal temperature variations ($\beta\to 0$, but $c_b=-\beta U_0$ finite). In this case, the temperature profiles are second order polynomials [$\overline{T}=\mathrm{Pr}c_b z^2/2-\Delta T z/2$, compare Eq. (4b)] leading to $S_{\mathrm{inv}}=1$ [12]. The thin lines are for Poiseuille flows ($\beta/v_m \ll 1$) with combined spatial and temporal variations of the boundary temperature, and are between those for pure (bold solid lines) and no (bold dashed lines) temporal temperature variations. In any case, Ra_c^u differs not more than 20% and k_c^u not more than 5% from the corresponding values for $U_0=0$ (bold dashed lines). These differences are small, considering that Ra^u varies very rapidly with ΔT (changing ΔT not only changes ΔT_u but also h_u, on which Ra^u depends quite sensitively). In order to explain the behavior of the thin lines for $h_u\to 0$, we note that in this limit $S_{\mathrm{inv}}\to 1$ for $\Delta T/(2\mathrm{Pr}\beta v_m)<-1$ and $S_{\mathrm{inv}}\to 0$ for $\Delta T/(2\mathrm{Pr}\beta v_m)=-1$ [13]. Therefore, the upper thin lines, where $\Delta T/(2\mathrm{Pr}\beta v_m)<-1$, approach the bold solid line, while the lower thin lines, where $\Delta T/(2\mathrm{Pr}\beta v_m)=-1$, approach the bold dashed lines for $h_u\to 0$.

The influence of the Prandtl number [which is equivalent to the influence of the term $\beta\overline{U}'$ on the eigenvalue problem (8a)–(8c)] is shown in Figs. 7 and 8. Here, the results derived above for Pr=7 (bold lines) are compared to those for $\mathrm{Pr}\to\infty$ (thin lines), i.e., when the β-$\overline{U}'$ coupling in Eq. (8a) can be neglected. The stability threshold for Couette flow (solid lines), which has $\beta\overline{U}'>0$ everywhere in the channel, is lowered by the β-$\overline{U}'$ coupling throughout, in agreement with our discussions above. For Poiseuille flow (long-dashed lines), on the other hand, $\beta\overline{U}'<0$ in the upper and $\beta\overline{U}'>0$ in the lower part of the channel, so that the destabilizing influence in the lower part of the channel may be largely compensated by the stabilizing influence in the upper part if h_u is large. Accordingly, the net destabilizing influence of this mechanism (i.e., the difference between the thin dashed and the bold dashed lines in the inset of Fig. 7) becomes noticeable only for sufficiently small h_u, when the bulk of the unstable layer is in the lower part. For the largely β-induced flow ($\beta/v_m=100$), $\beta\overline{U}'<0$ in the middle part and $\beta\overline{U}'>0$ near the boundaries of the channel [compare Fig. 2(a)]. Therefore, the influence of the β-$\overline{U}'$ coupling is stabilizing for large h_u (where a large part of the unstable layer is in the middle region) and becomes destabilizing for smaller h_u. This effect is shown in Fig. 8, where again the bold lines correspond to Pr=7 and the thin lines to $\mathrm{Pr}\to\infty$.

VI. CONCLUSION AND OUTLOOK

Although formally similar, the flows with conducting boundaries discussed here were found to behave in many respects quite differently from those with constant heat flux boundaries (see Ref. [6]). We have shown that the β-induced flow component may be either stabilizing or destabilizing, while for constant heat flux boundaries it is always stabilizing. Further, temporal variations in the boundary temperature corresponding to $U_0\neq 0$ were found to have the opposite effect as in the fixed boundary heat flux case. These results underline the different nature of these flows, which arise in quite a different context (see Sec. III B and Appendix).

The influence of the Prandtl number on the instability can be well described by a qualitative discussion of the β-$\overline{U}'$ coupling. While for very large Prandtl number this second instability mechanism has the character of a perturbation, it becomes increasingly important as Pr decreases. For very small Pr, also other velocity-dependent instability mechanisms are expected to become more relevant, since in that case larger velocities are required to sustain the same nonlinear vertical temperature profile [compare Eq. (4b)]. How these other modes are influenced by the horizontal temperature gradient is an important question for further research. The flows considered here may be particularly interesting in this context as their inflection point can be continuously shifted by varying β/v_m.

APPENDIX: BOUNDARIES WITH CONSTANT HEAT FLUX

We briefly discuss for constant heat flux boundaries the influence of temporal temperature variations (corresponding to $U_0\neq 0$) on the prefactor βv_m in Eq. (6). We only consider the case $\beta \ll v_m$, so that changes of the β-induced flow can be neglected. For this type of boundary condition, β is not imposed directly by the boundaries, but rather a result of the balance between heat advection and the net boundary heat flux $\Delta\Theta=\Theta_u-\Theta_l$, with $\Theta_u=T'(z=1)$ and $\Theta_l=T'(z=-1)$ being the heat flux at the upper and lower boundary, respectively.

Integrating Eq. (4b) from the lower to the upper boundary of the channel yields

$$\Delta\Theta = 2\mathrm{Pr}\beta(v_m-U_0)$$

or

$$\beta = \frac{\Delta\Theta}{2\mathrm{Pr}(v_m-U_0)}, \tag{A1}$$

which can be written as

$$\mathrm{Pr}\beta v_m = \frac{\Delta\Theta}{2}\left(1+\frac{U_0}{v_m-U_0}\right)$$

and

$$\mathrm{Pr}\beta U_0 = \frac{\Delta\Theta}{2}\left(\frac{U_0}{v_m-U_0}\right). \tag{A2}$$

Using Eq. (A2), $\beta \ll v_m$ and $\Delta T = -(\Theta_u + \Theta_l)$ (which is valid for $\beta \ll v_m$), we can now write Eq. (6) as

$$\overline{T}(z) = \frac{\Delta\Theta}{2}\left[T_p(z) + \frac{U_0}{v_m - U_0}\left(T_p(z) - \frac{z^2}{2} \right) + \frac{\Theta_u + \Theta_l}{\Delta\Theta} z \right]. \tag{A3}$$

We find that an increase of U_0 increases the contribution of the effective temperature component $T_p - z^2/2$ except for very large temporal changes of the temperature, when $U_0 > v_m$.

[1] J. W. Deardorff, Phys. Fluids **8**, 1027 (1965).

[2] For a review see R. E. Kelly, Adv. Appl. Mech. **31**, 35 (1994).

[3] J. E. Hart, J. Atmos. Sci. **29**, 687 (1972); J. E. Weber, J. Fluid Mech. **87**, 65 (1978); J. E. Hart, *ibid.* **132**, 271 (1983).

[4] For a brief overview of other work on such flows, see, e.g., T. M. Wang and S. A. Korpela, J. Fluid Mech. **87**, 65 (1992).

[5] W. Nakayama, G. J. Hwang, and K. C. Cheng, J. Heat Transfer **92**, 61 (1970); W. Akiyama, G. J. Hwang, and K. C. Cheng, *ibid.* **93**, 335 (1971).

[6] O. Stiller and W. Schöpf, Phys. Rev. Lett. **79**, 1674 (1997).

[7] The assumption of perfectly conducting boundaries is of course an idealized one. In an experiment, such boundaries are normally modeled by using a material that has a much (i.e., several orders of magnitude) larger thermal diffusivity than the fluid between the plates.

[8] The results for negative β are obtained by simultaneously changing the sign of the temperature and inverting z, which leaves the basic equations invariant.

[9] Note that the sign of ΔT_u has been chosen such that $\Delta T_u = T(z=-1) - T(z=-1+h_u)$ is positive, in accordance with the normal Rayleigh-Bénard problem.

[10] This temperature component includes the changes of βv_m that are induced by the temporal temperature variations corresponding to $U_0 \neq 0$, but not the changes of the vertical temperature profile caused by the β-induced flow component. The influence of U_0 on the β-induced flow depends strongly on v_m and therefore has to be considered separately.

[11] Note that for $h_u = 2$, the unstable layer extends over the whole channel height and the critical values approach those for normal Rayleigh-Bénard convection, which are exactly reproduced for $\beta v_m = \beta U_0 = 0$.

[12] For a quadratic temperature profile we can write $\partial_z \overline{T}(z) = \Theta_l - \mathrm{Pr}\beta U_0 (z+1)$. Then, $\partial_z \overline{T}(-1+h_u) = 0$ yields $h_u = \Theta_l / (\mathrm{Pr}\beta U_0)$ and thus $S_{\mathrm{inv}} = 1$.

[13] The limit $h_u \to 0$ corresponds to $U_0 / v_m \nearrow \Delta T / (2\mathrm{Pr}\beta v_m) + 1$, since the unstable layer vanishes for $U_0 / v_m \geqslant \Delta T / (2\mathrm{Pr}\beta v_m) + 1$ [see Eq. (7)]. Therefore, $\Delta T / (2\mathrm{Pr}\beta v_m) + 1 < 0$ and finite implies that U_0 / v_m remains finite with $U_0 / v_m < 0$, so that the quadratic term in Eq. (10) can be neglected for vanishing h_u. Hence, $\overline{T}(z)$ can be approximated by a second order polynomial leading to $S_{\mathrm{inv}} = 1$ and $S_{\mathrm{inv}} \to 1$ for $h_u \to 0$ [12]. If $\Delta T / (2\mathrm{Pr}\beta v_m) + 1 = 0$, on the other hand, Eq. (6) yields $\Theta_l = \mathrm{Pr}\beta U_0$ and thus $S_{\mathrm{inv}} = h_u$ which trivially tends to zero for $h_u \to 0$.